A New Numerical Integrator for Planet Formation

David Nesvorný[1]

Harold F. Levison[1]

ABSTRACT

We describe here a new numerical code that can be used for studies of planet formation. This code is based on SyMBA (Duncan et al. 1998), an efficient symplectic N-body integrator that uses a multiple time step algorithm in the Wisdom-Holman Map (Wisdom & Holman 1991). SyMBA is a valuable tool for the study of planet formation. It has, however, one fundamental limitation: the number of massive fully–interacting bodies that can be integrated with SyMBA using current CPUs is normally $\lesssim$1000. This number of bodies is low by many orders of magnitude to account for myriads of planetesimals participating in planetary accretion. We modified SyMBA to statistically account for the gravitational effects on planetary embryos of numerous small bodies. We projected two algorithms. In SyMBA-DFC1 (Dynamical Friction Code 1), small bodies are represented by a Sun-centered annulus with a continuous mass distribution; the dynamical friction effects (Chandrasekhar 1943) of this distribution on a massive object are calculated via the standard dynamical friction formula (e.g., Binney & Tremaine 1987). In SyMBA-DFC2 (Dynamical Friction Code 2), small bodies are represented by a 'tracer' test particle. When this particle encounters a massive body, the code calculates the impulse velocity change using the two-body approximation and impact parameters that are uniformly distributed on the target plane. SyMBA-DFC1/DFC2 can currently use up to ∼10,000 annuli/tracers to describe the orbital distribution of small bodies. These complementary codes will allow us to study effects of small bodies in the proto-planetary disks, which have been neglected in previous attempts to form the terrestrial planets (e.g., Chambers & Wetherill 1998, Agnor et al. 1999) despite the fact that numerous small planetesimals were present during the late stages of terrestrial planet accretion (Kokubo & Ida 2000). We have thoroughly tested the new simulators in models related to terrestrial planet formation and the early radial migration of the Jovian planets (Fernández and Ip, 1984). The new codes will also be useful to study the origin of the extrasolar planets.

---

[1]Southwest Research Institute, 1050 Walnut St, Suite 400, Boulder, CO 80302, USA

1. Introduction

Planets form via a 'bottom-up' process involving accumulation of small objects into larger ones. The planetary formation can be divided into three main phases. Each phase is characterized by its own unique set of physical conditions and important physical processes. In sketch form, these are:

1. *Early Stage:* This stage describes growth starting from microscopic particles (e.g., silicates and ices). It follows the evolution of these particles into larger and larger objects, and ultimately into planetesimals some 1 to 10 km across. During this stage, growth is controlled mainly by the dynamical interaction between the growing solid bodies and the gas disk in which they are embedded, mechanical sticking forces, and possible gravitational-thermal instabilities which may develop locally in the disk (see, e.g., Goldreich & Ward 1973, Weidenschilling & Cuzzi 1993).

2. *Middle Stage:* This stage follows the evolution of the myriad of kilometer-scale planetesimals as they grow into a number of roughly 1000-km scale protoplanets through accretionary collisions. This phase is one where the dynamical evolution of the system is relatively simple because growing embryos are not large enough to affect the system globally. However, collisions between objects are frequent and dominate the state of the system. Growth is increasingly controlled by a competition between the gravitational attraction that planetesimals exert on debris which impacts them and the energetics of the collisions which feed new mass onto the planetesimals. During this phase, theory has shown that the larger a body grows, the faster it grows, because its collisional cross section scales like its radius R to the 4th power (owing to its increasing gravitational influence). As a result, a 'runaway growth' phase eventually ensues (Greenberg et al. 1978, Wetherill & Stewart 1989), leading to a situation in which a relatively small number of protoplanetary 'embryos' (roughly 1000 km in diameter) grow to dominate any given region of a protoplanetary disk. These embryos remain embedded in a swarm of much smaller objects which serve as continued feedstock. Towards the end of this phase, the embryos become massive enough to largely perturb planetesimals in their feeding zones. The mass growth of the largest embryos then slows down (Kokubo & Ida 1998).

3. *Late Stage:* This stage commences when the planetary embryos become large enough to start to gravitationally affect each other and the state of the system. At this point, the system becomes very violent as the embryos gravitationally perturb each other into crossing orbits; generating titanic collisions in some cases, and in other cases, gravitationally hurling each other (and smaller objects) around the solar system. Most

of the embryos eventually collide with one another leading to the formation of the final planets (Weidenschilling et al. 1997, Chambers & Wetherill 1998, Agnor et al. 1999, Chambers 2001). The embryos also sweep up most of the remaining debris during this time. During this phase, the dynamical evolution is difficult to model, due to the large number of massive gravitationally-interacting bodies.

The present understanding of these processes has been discovered piecemeal, because the research community has only been able to design computer simulations that study the individual phases described above. No one has, as yet, been able to design a numerical experiment to study the very important transition between stages 1 and 2 or 2 and 3, owing in part to computational limitations, and in part to the fact that the three stages of planet formation are dominated by such different physical processes.

However, we know that this piecemeal modeling is not adequate, e.g., because models of the late-stage have been unable to reproduce the observed attributes of our own solar system. In the inner solar system, these models produce too few planets, and those that are formed are found on orbits that are too eccentric (Chambers & Wetherill 1998, Agnor et al. 1999, Chambers 2001). In the outer solar system, the models fail to form Uranus and Neptune in their present locations in the age of the solar system (cf. Stern et al. 1997, Levison & Stewart 2001). The most likely reason for this failures is that these models have started with naive initial conditions, ignored the role of small bodies, and inadequately handled collisions and interaction with the remnant gas nebula during the late stage.

To help this situation, we develop a new numerical code that statistically accounts for the effect of small bodies on growing embryos and handles collisions in more realistic ways than any previous N-body integrator. In this paper, we explain (section 2) and test (section 3) the algorithm that we use to follow the dynamical evolution of a planetesimal system. The collisional algorithm (adapted from Stern & Colwell 1997a,b) will be described elsewhere.

2. The New Code

Our code is based on SyMBA (Duncan et al. 1998, Levison & Duncan 2000). SyMBA is a symplectic algorithm that has the desirable properties of the sophisticated and highly efficient numerical algorithm known as Wisdom-Holman Map (WHM, Wisdom & Holman 1991) and that, in addition, can handle close encounters (Duncan et al. 1998). This technique is based on a variant of the standard WHM, but it handles close encounters by employing a multiple time step technique (Skeel and Biesiadecki 1994). When bodies are well separated, the algorithm has the speed of the WHM method, and whenever two bodies suffer a mutual

encounter, the time step for the relevant bodies is recursively subdivided.

Although SyMBA represented a significant advancement to the state-of-art of integrating orbits, it suffers from a basic and serious limitation. At each time step of the integration, it is necessary to calculate the mutual gravitational forces between all bodies in the simulation. If there are N bodies, one therefore requires N^2 force calculations per time step, because every objects needs to react to the gravitational force of every other body. Thus, even with fast clusters of workstations we are computationally limited to integrating systems where the total number of bodies is less than $\sim$1000.

Yet, in order to follow both the dynamical and collisional evolution of the numerous small bodies present during the middle and late stages of the formation of the solar system, we need to implement a way to follow the behavior of billions of particles. This clearly is beyond the capabilities of direct orbit integrators. With today's technology, only statistical methods can handle this number of objects. These methods have been pioneered by Safronov (1969) (see also Ohtsuki et al. (2002) for more recent references). In the following, we describe our approach to this problem.

At the end of the middle stage of planet formation, it has been shown that solar system objects follow a bimodal size distribution where there are a relatively small number of massive objects (known as embryos) and a very large number of much smaller, less massive objects (e.g., Greenberg et al. 1984, Kokubo & Ida 1996, 1998). Thus, it is natural to develop two classes of objects in SyMBA. The first class of objects will consist of the large, massive embryos. Since there are only a small number of these embryos, they can be followed dynamically, in the standard N-body part of the algorithm.

We also follow orbits of a *tracer* population of small objects. These tracer particles allow us to determine how the orbital distribution of small bodies evolves due to the gravitational effects of embryos. However, whereas each large embryo will represent a single real object, each single tracer will represent a large number of small bodies that are assumed to have the same orbital semimajor axis (a), eccentricity (e), and inclination (i). We have projected two codes. In the 1st code (SyMBA-DFC1), the longitudes of the ascending node (Ω), arguments of perihelion (ω), and mean anomalies (l) of small bodies associated to a tracer are assumed to be distributed randomly between 0 and 2π. In the 2nd code (SyMBA-DFC2), only l are randomly distributed. We describe these codes below.

2.1. SyMBA-DFC1

SyMBA-DFC1 (Dynamical Friction Code 1, hereafter DFC1) uses random distribution of Ω, ω, and l for small bodies. Such a distribution has the space number density (Kessler 1981, Sykes 1990):

$$P(r,\beta) = \frac{1}{2\pi^3 a^2 r} \frac{1}{\left[e^2 - \left(\frac{r}{a} - 1\right)^2\right]^{1/2} \left[\cos^2\beta - \cos^2 i\right]^{1/2}} \tag{1}$$

with the limits:

$$\begin{aligned} a(1-e) \leq \quad & r \quad \leq a(1+e) \ , \\ -i \leq \quad & \beta \quad \leq i \ . \end{aligned} \tag{2}$$

Here, $r = \sqrt{x^2+y^2+z^2}$, and $\beta = \arcsin(z/r)$, where x, y, z are the Cartesian coordinates. We normalized the above distribution to the total number of one body in the population. $P(r,\beta)\Delta x \Delta y \Delta z$ is then the probability that the body is located within a box $\Delta x \times \Delta y \times \Delta z$ centered at (x, y, z).

In Eq. 1, a, e and i are the orbital elements of the tracer particle. The velocity distribution at (x, y, z) of small bodies associated to this tracer particle is calculated from

$$\begin{aligned} v_x^2 + v_y^2 + v_z^2 &= 2\left(\mathcal{E} + \frac{k^2}{r}\right) \\ (yv_z - zv_y)^2 + (zv_x - xv_z)^2 &= \mathcal{M}^2 - \mathcal{M}_z^2 \\ xv_y - yv_x &= \mathcal{M}_z \ , \end{aligned} \tag{3}$$

where $\mathcal{E} = -k^2/2a$, $\mathcal{M} = k\sqrt{a(1-e^2)}$, and $\mathcal{M}_z = \mathcal{M}\cos i$ are the energy, angular momentum, and z-component of the angular momentum, respectively (all per unit mass). Here, $k = \sqrt{GM_*}$, where G is the gravitational constant, and M_* is the mass of the central star. In general, there are four solutions of Eq. (3) that give four velocity vectors $\vec{v}^{(i)} = (v_x^{(i)}, v_y^{(i)}, v_z^{(i)})$, $i = 1, \ldots, 4$, each of them corresponding to a specific orbital geometry. We calculate these velocity vectors by analytically solving Eq. (3). The final expressions for $\vec{v}^{(i)}$ (not shown here) represent only a small fraction of the CPU labor per time step.

Direct, symplectic integration of both the embryos and the tracer particles is performed via an N-body calculation, using the SyMBA algorithm, where the Sun and embryos all fully interact with each other. The tracer particles respond to the Sun, planets, and embryos, but do not gravitationally interact among themselves (this is an excellent approximation assuming that the dynamical stirring of the ensemble is dominated by encounters with the embryos, which seems to be the case during late stages of planet formation; Ida & Makino

1993). In addition, the code accounts for the effect of small bodies on embryos using the following recipe: (i) In time steps when the distance between a tracer and an embryo is large, we account for the gravitational effect of the tracer on the embryo normally, as if in the N-body integration; (ii) If, however, the tracer suffers a close encounter to the embryo, we switch off its direct gravitational effect on the embryo; (iii) Instead, we account for the combined effect on the embryo of all encounters of the small objects associated with the tracer (and all other tracers present in the simulation) at each time step elsewhere in the code. This is done using the following recipe.

We first check whether the massive body is located within the toroidal region populated by objects associated to one tracer (Eq. 2). If so, we assume that the massive body experiences two-body encounters with objects of this population. To evaluate the effect of these encounters, we calculate the change of the massive body's velocity using impulse approximation (e.g., Binney & Tremaine 1987, page 422). We iterate this procedure over all tracers.

If we define the relative velocity $\vec{w}$ as $\vec{w} = \vec{v} - \vec{u}$, where $\vec{v}$ and $\vec{u}$ are the velocities of bodies associated to the tracer and of the massive body, respectively, the change of $\vec{u}$ in a single encounter is:

$$\begin{aligned} (\Delta\vec{u})_{\perp} &= \frac{2mbw^3}{G(M+m)^2}\left[1+\frac{b^2w^4}{G^2(M+m)^2}\right]^{-1} \\ (\Delta\vec{u})_{\parallel} &= \frac{2mw}{G(M+m)^2}\left[1+\frac{b^2w^4}{G^2(M+m)^2}\right]^{-1} . \end{aligned} \tag{4}$$

The first equation shows the change of $\vec{u}$ in the direction perpendicular to $\vec{w}$. The second equation shows the change of $\vec{u}$ in the direction parallel to $\vec{w}$. $(\Delta\vec{u})_{\parallel}$ always points in the same direction as $\vec{w}$. b is the impact parameter, which is the minimum distance between the unperturbed trajectories (Öpik 1951). M and m are masses of the two bodies having encounter.

To determine the total velocity change (acceleration) of the massive body located at $\vec{r}$ and having velocity $\vec{u}$, we must sum the effects of all encounters with small bodies associated to the tracer. Mathematically, we must integrate Eq. (4) over the *target plane*. The target plane is centered at the massive body and is oriented normal to the unperturbed relative velocity $\vec{w}_{\infty}$. The integral is performed on b, from 0 to $b_{\rm MAX}$, where $b_{\rm MAX}$ is the maximum impact parameter. Encounters with $b > b_{\rm MAX}$ are ignored.

Figure 1 illustrates how the acceleration depends on $b_{\rm MAX}$. The two solid lines show accelerations computed by numerically integrating on the target plane over all encounters that occur within a distance $b_{\rm MAX}$ to the massive body. The resulting transversal acceleration

$(\mathrm{d}\vec{u}/\mathrm{d}t)_\perp$ is small, as expected, because of the symmetries. The principal effect of encounters is the acceleration parallel to $\vec{w}$. This effect is called the dynamical friction (Chandrasekhar 1943), because $(\Delta\vec{w})_\parallel$ always points in the direction opposite to $\vec{w}$.

We also note in Fig. 1 that $(\mathrm{d}\vec{u}/\mathrm{d}t)_\parallel$ is a strong function of b_{MAX} for small b_{MAX}, but when b_{MAX} is large ($\gtrsim 0.05AU$ which is $\approx$5 Hill spheres in this example), $(\mathrm{d}\vec{u}/\mathrm{d}t)_\parallel$ becomes nearly independent of b_{MAX}. Our additional tests have shown that it is generally good enough (to $\sim$10% accuracy) to take b_{MAX} about a factor of 5–10 larger than the Hill radius of massive body, assuming the disk of small bodies extends so far.

Numerical integrations over the target plane are CPU-time consuming. An algorithm based on such a procedure would be very slow. For this reason, we expand $P(x,y,z)$ and $\vec{v}(x,y,z)$ in Taylor series around the location of the massive body, and analytically integrate the second equation in Eq. (4) over the target plane. If only the 1st term of the expansion is taken into account, the resulting expression is:

$$\frac{\mathrm{d}\vec{u}}{\mathrm{d}t} = 2\pi P(r,\beta)G^2 m(M+m)\sum_{i=1}^{4}\left[\ln(1+\Lambda^2)\frac{\vec{w}^{(i)}}{(w^{(i)})^3}\right] \ , \tag{5}$$

where

$$\Lambda = \frac{b_{\mathrm{MAX}}(w^{(i)})^3}{G(M+m)} \ . \tag{6}$$

Here, $\vec{w}^{(i)} = \vec{v}^{(i)} - \vec{u}$, where $\vec{v}^{(i)}$ are the four velocities determined from Eq. (3).

The dashed line in Fig. 1 shows the acceleration $(\frac{\mathrm{d}\vec{u}}{\mathrm{d}t})_\parallel$ computed from Eq. (5). The logarithmic dependence of $(\frac{\mathrm{d}\vec{u}}{\mathrm{d}t})_\parallel$ on b_{MAX} (see Eq. 5) closely follows the acceleration evaluated numerically, which hints on practical applicability of the analytical averaging. In general, Eq. (5) proves to be a very good approximation of the interaction term parallel to $\vec{w}^{(i)}$, and we use it in the DFC1.

One limitation of the analytic averaging occurs when the massive body moves close to the border of the toroidal region populated by objects associated to some tracer. In such a case, the acceleration evaluated from Eq. (5) may be in error, because of the large local gradients of $P(r,\beta)$. Our tests show, however, that this is not a crucial limitation of the algorithm (section 3).

Another nice aspect of the Eq. (5) is that it allows us to understand in simple terms how the dynamical friction effects depend on masses of interacting bodies. If we assume that M and $f(m)$ are the mass of the large embryo and the mass distribution of small planetesimals, Eq. (5) should be integrated over m to yield the total $\mathrm{d}\vec{u}/\mathrm{d}t$. If we ignore the

weak logarithmic dependence on mass through Λ, the relevant term is:

$$\int_{m'} f(m')m'(M+m')\mathrm{d}m' = m\left(M + \frac{\langle m^2\rangle}{\langle m\rangle}\right) \ , \tag{7}$$

where m, $\langle m\rangle$, and $\langle m^2\rangle$ are the total, average, and average square masses of planetesimals, respectively. It is thus obvious that the dynamical friction effects do not depend on the individual masses of planetesimals, but only on their total mass m, if $M \gg \langle m\rangle$.

2.2. SyMBA-DFC2

In our 2nd code (SyMBA-DFC2, Dynamical Friction Code 2, hereafter DFC2), the planetesimal's mass is set to zero during a close encounter with the planet. The impact parameter, and the asymptotic relative velocity that characterize its encounter are then used to analytically compute the impulse velocity change that the planet would suffer if it encountered a beam of infinitesimal particles, with total mass equal to that of the parent planetesimal and essentially the same incoming orbit. In particular, the asymptotic relative velocity vector of the beam particles is the same as recorded for the parent planetesimal, and the impact parameters are uniformly distributed on the target plane (the plane that passes through the planet's position and is orthogonal to the asymptotic relative velocity vector) within 3 Hill radii from the planet's position.

3. Tests

We test the DFC1 and DFC2 in several models related to terrestrial planet formation (sections 3.1–3.4) and the early radial migration of the Jovian planets (section 3.5). The purpose of these tests is to check whether our codes can correctly follow the dynamical interaction of planetesimals and proto-planets during different phases of planet formation. We use collision-less systems in these tests (i.e., we neglect the collision cross-section of simulated bodies) because we want to focus on *dynamical* evolution. These experiments are described below. Our collisional algorithm was adapted from Stern & Colwell (1997a,b) and will be described elsewhere (Stern et al., in preparation).

3.1. Earth-mass planet embedded in a planetesimal disk

To deal separately with the dynamical friction effects described by Eq. (5) and the long-distance perturbations, we first run a series of tests where planetesimals do not perturb

proto-planets except through the dynamical friction term (Eq. 5). Effects of the long-distance (secular) perturbations are included in similar tests in the next section.

We randomly distribute one hundred tracer particles in an annulus around an 1 $M_\odot$ star with $0.95 \leq a \leq 1.05$ AU. The total mass in the annulus is set to $M_\oplus$. We place an $M = M_\oplus$ protoplanet in the center of this annulus (at $a_{\rm M} = 1$ AU) with $i_{\rm M} = 0$, and use several eccentricity values $e_{\rm M}$ to test the dependence of the dynamical friction on eccentricity. Because we want to cancel the secular effects on the protoplanet, we distribute the initial eccentricities e and periapse longitudes ϖ of the tracer particles so that $e\cos\varpi = e_{\rm M}\cos\varpi_{\rm M} + e_{\rm prop}\cos\varpi_{\rm prop}$, and $e\sin\varpi = e_{\rm M}\sin\varpi_{\rm M} + e_{\rm prop}\sin\varpi_{\rm prop}$, where $e_{\rm M}$ and $\varpi_{\rm M}$ are the initial eccentricity and periapse longitude of the protoplanet, $\varpi_{\rm prop}$ are uniformly distributed between 0 and π, and $e_{\rm prop}$ have the Rayleigh distribution (Ida & Makino 1992) with RMS proper $e = \sqrt{\langle e_{\rm prop}^2\rangle} = 0.1$. See Murray & Dermott (1999) for definition of proper (or 'free') elements. Here and in the following, $\langle\cdot\rangle$ denotes average. The initial inclinations of tracer particles have the Rayleigh distribution with RMS $i = \sqrt{\langle i^2\rangle} = 0.1$. We follow this system for 10^5 years with a 0.01 yr time step using the DFC1 & 2.

For a reference, we also follow the evolution of $M = M_\oplus$ protoplanet embedded in a disk of 1000 point-mass planetesimal using the N-body code SyMBA. The total mass and the initial distribution of these planetesimals are the same as in above.

In both the test and reference cases, we moreover assign a non-zero second zonal coefficient J_2 to the central star. This is required for correct comparison. Note that there does not exist any mechanism to rotate orbital apses in the test case, because long-distance effects on the protoplanet are switched off. In the reference experiment, the assumed value of J_2 speeds up the rotation of apses by about a factor of two with respect to the situation where the apses secularly rotate solely under the influence of the disk.

In Fig. 2, we show a comparison between the test (100 tracers and DFC1) and reference (1000 disk particles and SyMBA) evolutions for four initial eccentricities of the protoplanet. The effect of dynamical friction on these evolutions is evident: eccentricity of the massive protoplanet decays in all cases. On the other hand, the disk particles receive higher e because the protoplanet stirs their orbits. The agreement between test and reference integrations is good showing that the DFC1 includes all important dynamical interactions of the protoplanet with the disk. Fig. 3 shows the same comparison as Fig. 2b, but for the DFC2. Also in this case, the agreement is good.

To push things to limits, we wanted to know what is the minimum number of tracers that have to be used to resolve the protoplanet-disk interaction with the DFC1 & 2. It turns out that with 20 tracers, both the DFC1 and DFC2 produce evolutions that are in a

reasonable agreement with the reference case (Fig. 4). Conversely, with only five tracers, the orbital evolution of the protoplanet becomes very irregular. This tells us that $\gtrsim$10 tracers should be used per radial 0.1 AU of the disk in applications where the DFC1 & 2 are used to simulate late stages of terrestrial planets' formation. For comparison, Chambers (2001) used 140 point-mass bodies ($\sim 0.01 M_\oplus$ each) to resolve the planetesimal disk at 0.3–2 AU.

3.2. Secular friction

Tests of the DFC1 & 2 presented in this section are similar to those described in the previous section. Instead of neglecting the long-distance interactions, however, we will now account for the full interaction of the protoplanet with the planetesimal disk using the algorithm described in section 2. As before, we test DFC1 & 2 using the 1 $M_\oplus$ protoplanet $a = 1$ AU that is embedded in the 1 $M_\oplus$ disk of planetesimals at $0.95 \leq a \leq 1.05$ AU. Only this time, the initial ϖ and e of planetesimals are not displaced by $\varpi_{\rm M}$ and $e_{\rm M}$, but are selected randomly according to uniform and Rayleigh distributions, respectively.

In Fig. 5, we show a comparison between the test (100 tracers and DFC1) and reference (1000 disk particles and SyMBA) evolutions for four different initial eccentricities of the protoplanet. The evolutions shown in Figs. 5a & b are not very different from the ones in Figs. 2a & b, where secular effects were neglected. In contrast, the evolutions that started with higher e of the protoplanet ($e = 0.1$ and 0.14 in Figs. 5c & d) show trends unlike those in Figs. 2c & d. The eccentricity of the protoplanet rapidly drops to low values at $t < 10^4$ yr, then oscillates with a large amplitude, and eventually evolves to very low values (compare $e = 0.01$–0.02 at $t = 10^5$ yr in Figs. 5c & d to $e = 0.03$–0.07 at $t = 10^5$ yr in Figs. 2c & d). This behavior of e surges from the dynamical evolution of the system toward a secular equilibrium. It can be explained in terms of the classical secular theory.

For simplicity, assume that a protoplanet of mass M moves around the central star in an orbit that is coplanar with the planetesimal disk of mass $M_{\rm disk}$. If $M \gg M_{\rm disk}$, orbital motion of each small planetesimal in the disk is controlled by the massive protoplanet. The secular evolution of each planetesimal's e and ϖ can then be represented by a vector of constant length (equal to $e_{\rm prop}$ or 'free' eccentricity; see, e.g., Murray & Dermott 1999) in the $e\cos\varpi, e\sin\varpi$ plane that rotates with a constant angular speed around (x, y) (Fig. 6a). Location of the center of these rotations (x, y) is determined by the so-called 'forced' secular term. In general, $(x, y) = (e_{\rm f}\cos\varpi_{\rm f}, e_{\rm f}\sin\varpi_{\rm f})$, where $e_{\rm f}$ and $\varpi_{\rm f}$ are the forced eccentricity and forced periapse longitude. These quantities are functions of M, $e_{\rm M}$, $\varpi_{\rm M}$, and a. For $a \sim a_{\rm M}$, where $a_{\rm M}$ is the semimajor axis of the protoplanet ($|a - a_{\rm M}| < 0.05$ AU in our tests), $(x, y) \approx (e_{\rm M}\cos\varpi_{\rm M}, e_{\rm M}\sin\varpi_{\rm M})$.

A protoplanet that forms in the disk acts on the disk planetesimals in such a way that it pushes their e to values on average larger than its own (Fig. 6b). By reaction, because this process involves transfer of the angular momentum, the protoplanet's e must drop. This is what happens at $t < 10^4$ yr in Fig. 5c & d, but does not in Fig. 2c & d, where secular interactions are absent. When the new secular equilibrium is reconstituted, planetesimals have on average larger eccentricities then they had initially, and their periapses tend to be aligned with $\varpi_{\rm f}$. Because the protoplanet's eccentricity decays, we name this effect 'secular friction'. The secular friction also affects inclinations of protoplanets which orbits are tilted with respect to the planetesimals' disk mid-plane.

The secular friction was originally described by Tremaine (1998). He argued that secular effects control the evolution of dynamically 'hot' disks (i.e., $e \sim i \gtrsim 0.1$). In cold, self-gravitating disks, the secular friction manifests itself by spiral density waves that are launched in the disk at resonant locations (Goldreich & Tremaine 1980). In effect, the protoplanets e also decays (Ward 1988, Agnor & Ward 2002). The transfer of orbital angular momentum from protoplanets to the primordial particulate and/or gas disks may be fundamental to explain today's low value of the Angular Momentum Deficit (Laskar 2000) of the terrestrial planets.

In closing this section we conclude that the DFC1 & 2 (see Fig. 7) can correctly follow the dynamical interaction of protoplanets with planetesimal disks. Until know, however, we only focused on effects on the eccentricity in dynamically 'hot' disks (i.e., $e \sim i \sim 0.1$). In the next section, we will test the behavior of inclinations. In section 3.4, we will test the codes using dynamically 'cold' disks in models that are relevant for the early stages of planet formation.

3.3. Effects on i

To test the behavior of inclination that results from the interaction of a protoplanets with a planetesimal disk, we randomly distribute one hundred tracer particles in an annulus around an 1 $M_\odot$ star with $0.95 \leq a \leq 1.05$ AU, with e and i according to the Rayleigh distribution, and $\sqrt{\langle e^2 \rangle} = 0.1$ and $\sqrt{\langle i^2 \rangle} = 0.05$. We place the protoplanet in the center of this annulus (at $a = 1$ AU) with $e = i$, and use several values of i to test the dependence of dynamical effects on inclination. As in above, the total mass in the annulus and the mass of the protoplanet are both set to $M_\oplus$. In addition, we account for the gravitational perturbations by a Jupiter-mass planet that is assumed to have a circular orbit at 5.2 AU, and neglect J_2 of the central star. We follow the system for 10^5 years with a time step of 0.01 yr.

In Fig. 8, we show a comparison between the test (DFC1 – top panels, DFC2 – bottom panels) and reference (1000 disk particles and SyMBA) evolutions for two different initial inclinations of the protoplanet. For $i = 5°$ (left panels in Fig. 8), the inclination of the protoplanet oscillates with large amplitude due to the secular interactions with the disk, and eventually reaches an equilibrium value of about 2.8° (0.05 radians) at $t = 10^5$ yr. Both the DFC1 & 2 reproduce the reference evolutions reasonably well. For $i = 1°$ (right panels in Fig. 8), however, the DFC1 fails to match the reference case because it dumps the protoplanet's i to near-zero values while in the reference evolution, the initial and final values of the protoplanet's i are similar. The origin of this behavior is unknown [NEEDS TO BE EXPLAINED AND CORRECTED]. On the other hand, the DFC2 shows a good agreement with reference integrations in all tests.

In Fig. 9, we finally check the evolutions of i calculated by the DFC1 (top panels in Fig. 9) and by the DFC2 (bottom panels) in simulations where the planetesimal disk is represented by 20 (left panels of Fig. 9) and 5 tracers (right panels). It turns out that with 20 tracers, the general trends of these evolution are similar to the ones produced by the reference simulation, but things like the wavelength of the secular oscillations may slightly differ. With only five tracers, the orbital evolutions become very irregular. As in section 3.2, also here we find reasons to believe that $\gtrsim$10 tracers should be used per radial 0.1 AU of the disk in applications where the DFC1 & 2 are used to simulate late stages of terrestrial planets' formation.

3.4. Comparison with Ohtsuki et al.

Here we test the DFC1 & 2 in situations where orbits are more circular and less inclined than in our previous tests, and where the planetary embryos have masses that are only a small fraction of $M_\oplus$. We take these tests from Ohtsuki et al. (2002).

Ohtsuki et al. calculated the rates of evolution of the RMS eccentricity ($\sqrt{\langle e^2 \rangle}$), and the RMS inclination ($\sqrt{\langle i^2 \rangle}$) in planetesimal disks. These evolutions are driven by distinct physics depending on whether the planetesimal disk is dynamically 'cold' or dynamically 'hot' (see also Ida 1990, Wetherill and Stewart 1989, 1993, Stewart and Ida 2000). As a result, the rates of evolution $\mathrm{d}\sqrt{\langle e^2 \rangle}/\mathrm{d}t$ and $\mathrm{d}\sqrt{\langle i^2 \rangle}/\mathrm{d}t$ take different functional forms in parameters like the planetesimals' mass distribution, $\sqrt{\langle e^2 \rangle}$, and $\sqrt{\langle i^2 \rangle}$ in limits of hot and cold disks. For example, $|\mathrm{d}\sqrt{\langle e^2 \rangle}/\mathrm{d}t| \gg |\mathrm{d}\sqrt{\langle i^2 \rangle}/\mathrm{d}t|$ in the cold disk limit, while $\sqrt{\langle i^2 \rangle} \approx 0.5\sqrt{\langle e^2 \rangle}$ is spontaneously attained in dynamically hot Keplerian disks (Ida 1990, Ida and Makino 1992b).

In the 'dispersion-dominated' limit (hot disk), the overall dynamical evolution of the system can be described by a sequence of hyperbolic two–body encounters. Each single encounter between two planetesimals rotates their velocity vectors thus almost instantaneously changing their orbital momentum (Öpik 1951, Valsecchi et al. 1997). Statistically, the effect of numerous such encounters can be determined from Eq. (5). We thus realize that our code, which uses Eq. (5), can be used to follow the dynamical evolution of protoplanets and planetesimals in the hot disks limit. We verified this using tests related to the late stages of terrestrial planet formation in sections 3.1–3.3

In the 'shear-dominated' dominated regime (cold disk), three-body effects during typical encounters between two planetesimals become important. Planetesimals evolve via orbital paths that are solutions of the Hill's equations (e.g., Hénon & Petit 1969). Temporary pairs of gravitationally bound bodies are formed frequently; the redistribution of orbital energy and momentum during these interactions can be complex. Our code can not handle this situation, because these interactions are not described by Eq. (5).

How do we know whether the proto-planetary disk is dynamically hot or cold? To define these regimes, we compare the magnitude of the Kepler-shear velocity with the one of random velocities of planetesimals in the disk arising from their non-zero e and i. The Kepler-shear velocity is conveniently characterized by the Hill velocity, $V_{\rm H}$, which is the differential Kepler velocity between two bodies on co-planar circular orbits that have the radial separation equal to one mutual Hill radius, $R_{\rm H}$, where

$$R_{\rm H} = a \left(\frac{m_1 + m_2}{3M_*} \right)^{\frac{1}{3}} \quad . \tag{8}$$

Here, a is the semimajor axis, m_1, m_2, and M_* are the masses of the two bodies and of the central star, respectively. The Hill velocity is then:

$$V_{\rm H} = \frac{1}{2} \frac{\sqrt{GM_*}}{a^{3/2}} R_{\rm H} = \frac{1}{2} V_{\rm K} \left(\frac{m_1 + m_2}{3M_*} \right)^{\frac{1}{3}} \quad , \tag{9}$$

where G is the gravitational constant, and $V_{\rm K} = \sqrt{GM_*/a}$ is the Keplerian velocity at the semimajor axis a.

The random velocity, $V_{\rm R}$, is the typical encounter velocity in a system of planetesimals that have eccentricities e end inclinations i. For small values of e and i,

$$V_{\rm R} \approx V_{\rm K} \sqrt{e^2 + i^2} \ , \tag{10}$$

where $i \ll e$ in the cold disk limit, and $i \approx 0.5e$ in the hot disk limit (e.g., Ida and Makino 1992a).

The random-velocity dominated regime (hereafter dispersion-dominated regime) can be defined by $V_{\rm R} \gtrsim 4V_{\rm H}$ (e.g., Ohtsuki et al. 2002). By substitution from Eqs. 10 and 9, this condition becomes:

$$\sqrt{e^2+i^2} \gtrsim 2\left(\frac{m_1+m_2}{3M_*}\right)^{\frac{1}{3}} \quad . \tag{11}$$

If this condition is satisfied, the three-body effects during encounters can be neglected. To test this, we conduct a series of numerical experiments, where we calculate the rates of evolution of e and i in the collisionless planetesimal systems using the DFC1 & 2, and compare the results to the rates of evolution of e and i obtained by using the exact N-body code SyMBA.

The initial setup for these experiments were taken from the example given by Ohtsuki et al. (2002, see also Stewart & Ida 2000). These authors used the N-body integrator and a special-purpose hardware, GRAPE-4 (Makino et al. 1997), to numerically integrate the evolution of system of 1000 planetesimals over 1000 years. In our experiment, we used their two-component system (Fig. 4b in Ohtsuki et al. 2002), where 200 big planetesimals ($m_1 = 4 \times 10^{24}$ g) and 800 small planetesimals ($m_2 = 10^{24}$ g) are initially distributed at 1 AU around an 1 $M_\odot$ star with the total surface density of 10 g cm^{-2}. Initial e and i of these bodies were assumed to have the Rayleigh distribution with $\sqrt{\langle e^2 \rangle} = 10^{-4}$ and $\sqrt{\langle i^2 \rangle} = 5 \times 10^{-5}$. To resolve the disk of small bodies with DC1 & 2, we use 200 tracers with $m = 4 \times 10^{24}$ g each.

This two-component system is dynamically cold because $4V_{\rm H}/V_{\rm K} \approx 2{\times}10^{-3} > \sqrt{\langle e^2 \rangle + \langle i^2 \rangle}$. For test purposes, we thus use higher initial values of the RMS eccentricity and RMS inclination of the simulated planetesimals: $\sqrt{\langle e^2 \rangle} = 2 \times 10^{-4}$, 5×10^{-4}, 10^{-3}, 2×10^{-3}, and 5×10^{-3}, with $\sqrt{\langle i^2 \rangle} = 0.5\sqrt{\langle e^2 \rangle}$ in all cases. Figure 10 shows the evolutions of $\sqrt{\langle e^2 \rangle}$ and $\sqrt{\langle i^2 \rangle}$ computed by the DFC1 (solid lines) and by the exact N-body code SyMBA (dashed lines) for these five initial values of $\sqrt{\langle e^2 \rangle}$ and $\sqrt{\langle i^2 \rangle}$.

For systems started in the shear-dominated regime (i.e., $\sqrt{\langle e^2 \rangle + \langle i^2 \rangle} \lesssim 2 \times 10^{-3}$), the RMS eccentricity of both the small and big bodies rapidly increases since $t = 0$ ($e \propto t^2$) to reach values of $\sim 4 \times 10^{-3}$ at $t = 1000$ yr. In contrast, the RMS inclination increases slowly during the initial epochs, and faster during the late epochs, to reach values $\sim 2 \times 10^{-3}$ at $t = 1000$ yr. This evolution is predicted by theory because $|{\rm d}\sqrt{\langle e^2 \rangle}/{\rm d}t| \gg |{\rm d}\sqrt{\langle i^2 \rangle}/{\rm d}t|$ in the cold disk limit, while $\sqrt{\langle i^2 \rangle} \approx 0.5\sqrt{\langle e^2 \rangle}$ is typical for the relaxed, dispersion-dominated disks (Ida 1990, Ida & Makino 1992a).

The evolutions determined by the DFC1 (solid lines) agree within 10% with the results of the N-body code for all initial $\sqrt{\langle e^2 \rangle}$ including those started in the shear-dominated regime (i.e., $\sqrt{\langle e^2 \rangle + \langle i^2 \rangle} < 2 \times 10^{-3}$). This may seem surprising provided that the physics

of the three-body interactions is *not* accounted for in the DFC1. We explain this agreement by using results of the statistical theory (e.g., Ohtsuki et al. 2002).

We first note that if the big and small bodies have the same surface densities ($\Sigma = \sigma = 5$ g cm^{-2} in our tests), the viscous stirring from the big bodies is a factor of $\sim m_1/m_2 = 4$ more important than the viscous stirring from the small bodies (follows from Eq. 6 in Ohtsuki et al., see also Ida & Makino 1993). We can thus grossly neglect the self-gravity of small bodies. Second, the ratio of the rate of viscous stirring among the big bodies to the rate of the dynamical friction from small bodies is roughly $\Sigma\langle P\rangle_{\rm VS}/\sigma\langle P\rangle_{\rm DF}$, where $\langle P\rangle_{\rm VS}$ and $\langle P\rangle_{\rm DF}$ are coefficients defined by Eq. (6) in Ohtsuki et al. (see also Ida 1990, Stewart & Ida 2000). It turns out that $\langle P\rangle_{\rm VS} \gg \langle P\rangle_{\rm DF}$ in the sheer-dominated regime. Taken together, the rate of viscous stirring among the big bodies is this much larger than viscous stirring and dynamical friction effects from the small body population for $\sqrt{\langle e^2\rangle + \langle i^2\rangle} < 2 \times 10^{-3}$. This explains why the evolution paths determined by the DFC1 are similar to those calculated using the N-body code (Fig. 10). Indeed, the dynamical stirring by the large bodies, which the most important effect in the studied regime, is followed by a deterministic N-body code in the DFC1 (section 2).

Based on this result, we conclude that our new codes can be used for studies of cold proto-planetary disks if two conditions are satisfied: (i) $\Sigma/\sigma \gg \langle P\rangle_{\rm DF}/\langle P\rangle_{\rm VS} \sim 10^{-2}$ to neglect the effect of dynamical friction, and (ii) $\Sigma M/\sigma m \gg 1$ to neglect the effect of small bodies' self-gravity, where M and m are the typical masses of big and small bodies, respectively. In practice, we must choose some critical mass $M_{\rm crit}$ and group bodies into two categories: big ($M > M_{\rm crit}$) and small ($M < M_{\rm crit}$). $M_{\rm crit}$ must be chosen so that the number of big bodies N is as large as possible (in the range allowed by the CPUs used) to satisfy the above conditions. This is apparently easier for planetesimal populations characterized by steep mass distributions where most of the mass is in the big bodies, and is less likely to work for populations with shallow mass distributions (i.e., when most mass is in smallest bodies).

Transition of the system from the shear– to dispersion–dominated regime may present an additional problem, because $\langle P\rangle_{\rm DF}$ and $\langle P\rangle_{\rm VS}$ become comparable (e.g., Ohtsuki et al. 2002). In such a situation, the DFC1 & 2 can be used only if $\Sigma/\sigma \gtrsim 1$. It is unclear, however, whether this strict condition is actually required, because once the system enters the dispersion-dominated regime, the DFC1 & 2 can calculate the effects of dynamical friction correctly.

We now test the new codes in the dispersion-dominated regime. We use the same two-component system of planetesimals as above, only this time we use larger initial $\sqrt{\langle e^2\rangle}$ and $\sqrt{\langle i^2\rangle}$ ($2\sqrt{\langle i^2\rangle} = \sqrt{\langle e^2\rangle} = 5 \times 10^{-3}$, 10^{-2} and 5×10^{-2}), We also use longer integration

time span (10^4 years), because planetesimals now occupy larger volume and their dynamical evolution is slow.

Figure 11 shows the result. Because not much evolution happened with $\sqrt{\langle e^2 \rangle} = 5 \times 10^{-2}$ over 10^4 years, we focus on two cases started with lower $\sqrt{\langle e^2 \rangle}$. The test and reference evolutions shown in Fig. 11 are similar. The difference seen, for example, between the test and reference evolutions of $\sqrt{\langle e^2 \rangle}$ of the large planetesimals for $\sqrt{\langle e^2 \rangle} = 5 \times 10^{-3}$, is generated by stochastic interactions in the system. In fact, two integrations conducted with the same N-body integrator produce different reference evolutions when slightly different time steps are used. Exact comparison is thus difficult, unless we re-do the same runs several times and compare the 'average' solutions. This seems to be unnecessary. According to our additional tests, the agreement between the DFC1, the DFC2, and the N-body SyMBA code is satisfactory.

4. Conclusions

Here we described a computer code that will allow us to study the middle and late stages of planet formation. This code symplectically integrates the N-body dynamics of the large objects which grow by collisions from the small body population, and also statistically handles the gravitational perturbations between large and small objects. This code is unique, because unlike previous codes used to simulate the late stage of planet formation, it allows us to account for the fundamental effect known as dynamical friction (Chandrasekhar 1943). The dynamical friction occurs when a massive body penetrates into a swarm of small bodies and gravitationally interacts with them during close encounters. The net effect of this interaction is that the massive body gradually decelerates as if suffering a friction. In the context of planet formation, this means that the eccentricities and inclinations of the massive embryos become small by interaction with numerous small planetesimals.

Another important effect that can control the evolution of planetary embryos that are embedded in a dynamically hot disk is the secular friction (Tremaine 1998). In particular, we found that the late stages of planet formation can be best described as series of two-body encounters between the planetary embryos when these bodies accrete or scatter from each other. Every one of these interactions is then followed by evolution of the system toward a new secular equilibrium. Taken together, these evolutions produce a sort of secular friction where orbital momentum is transferred from orbits of the large bodies into the orbital motion of small bodies. This mechanism can be fundamental to explain the nearly circular and coplanar orbits of the terrestrial planets.

To model planet formation, our dynamical friction codes need to realistically account for mergers and fragmentations that occur when objects collide. Our approach to this problem is based on Stern & Colwell (1997a,b) and will be described in Stern et al. (in preparation). Moreover, the codes have been modified to account for the drag effect on planetesimals from the primordial gas nebula (Adachi et al. 1976). The gas drag can decrease e and i of small planetesimals thus effectively increasing the effects of dynamical and secular frictions on large planetary embryos. It can also increase sizes of the feeding zones of the planetary embryos.

An interesting additional issue is whether we can use Eq. 4 to account for effects of viscous stirring in disks of small self-gravitating planetesimals. In principle, this may be possible if we account for local gradients of $P(r, \beta)$ (Eq. 2) and $\vec{v}$ (Eq. 3). The transversal component of $\Delta\vec{v}$ in Eq. 4 will then have a non-zero contribution to the acceleration and will mimic the viscous stirring effects among the small planetesimals.

REFERENCES

Agnor, C.B., R.M. Canup, and H.F. Levison 1999. On the Character and Consequences of Large Impacts in the Late Stage of Terrestrial Planet Formation. *Icarus* **142**, 219–237.

Binney, J., and S. Tremaine 1987. Galactic Dynamics (J.P. Ostriker, ed.), Princeton University Press, Princeton, New Jersey.

Chambers, J.W., and G.W. Wetherill 1998. Making the Terrestrial Planets: N-Body Integrations of Planetary Embryos in Three Dimensions. *Icarus* **136**, 304–327.

Chambers, J.E. 2001. Making More Terrestrial Planets. *Icarus* **152**, 205–224.

Chandrasekhar, S. 1943. *Astrophys. J.* **97**, 255.

Duncan, M.J., H.F. Levison, and M.H. Lee 1998. A Multiple Time Step Symplectic Algorithm for Integrating Close Encounters. *Astron. J.* **116**, 2067–2077.

Greenberg, R., S.J. Weidenschilling, C.R. Chapman, and D.R. Davis 1984. From Icy Planetesimals to Outer Planets and Comets. *Icarus* **59**, 87.

Goldreich, P., and W.R. Ward 1973. The Formation of Planetesimals. *Astrophys. J.* **183**, 1051–1061.

Ida, S. 1990. Stirring and Dynamical Friction Rates of Planetesimals in the Solar Gravitational Field. *Icarus* **88**, 129–145.

Ida, S., and J. Makino 1992a. N-Body Simulation of Gravitational Interaction between Planetesimals and a Protoplanet. I. Velocity Distribution of Planetesimals. *Icarus* **96**, 107–120.

Ida, S., and J. Makino 1992b. N-Body Simulation of Gravitational Interaction between Planetesimals and a Protoplanet. II. Dynamical Friction. *Icarus* **98**, 28–37.

Ida, S., and J. Makino 1993. Scattering of Planetesimals by a Protoplanet: The Slowing Down of Runaway Growth. *Icarus* **106**, 210–227.

Kessler, D.J. 1981. Derivation of the Collision Probability between Orbiting Objects: The Lifetimes of Jupiter's Outer Moons. *Icarus* **48**, 39–48.

Kokubo, E., and S. Ida 1995. Orbital Evolution of Protoplanets Embedded in a Swarm of Planetesimals. *Icarus* **114**, 247–257.

Kokubo, E., and S. Ida 1996. On Runaway Growth of Planetesimals. *Icarus* **123**, 180–191.

Kokubo, E., and S. Ida 1998. Oligarchic Growth of Protoplanets. *Icarus* **131**, 171–178.

Kokubo, E., and S. Ida 2000. Formation of Protoplanets from Planetesimals in the Solar Nebula. *Icarus* **143**, 15–27.

Levison, H. F., and M. Duncan 2000. Symplectically Integrating Close Encounters with the Sun. *Astron. J.* **120**, 2117–2123.

Levison, H.F., and G.R. Stewart 2001. Remarks on Modeling the Formation of Uranus and Neptune *Icarus* **153**, 224–228.

Namouni, F., J.F. Luciani, and R. Pellat 1996. The Formation of Planetary Cores: a Numerical Approach. *Astron. Astrophys. 307*, 972–980.

Ohtsuki, K. 1999. Evolution of Particle Velocity Dispersion in a Circumplanetary Disk Due to Inelastic Collisions and Gravitational Interactions. *Icarus* **137**, 152–177.

Ohtsuki, K., G.R. Stewart, and S. Ida 2002. Evolution of Planetesimal Velocities Based on Three-Body Orbital Integrations and Growth of Protoplanets. *Icarus* **155**, 436–453.

Öpik, E.J. 1951. Collision Probabilities with the Planets and the Distribution of Interplanetary Matter. *Proc. Roy. Irish Acad.* **54**, 165–199.

Skeel, R.D., and J.J. Biesiadecki 1994. Symplectic Integration with a Variable Stepsize. *Ann. Numer. Math.* **1**, 1–9.

Stern, S.A., and J.E. Colwell 1997a. Accretion in the Edgeworth-Kuiper Belt: Forming 100–1000 Km Radius Bodies at 30 AU and Beyond. *Astron. J.* **114**, 841–849.

Stern, S.A., and J.E. Colwell 1997b. Collisional Erosion in the Primordial Edgeworth-Kuiper Belt and the Generation of the 30–50 AU Kuiper Gap. *Astron. J.* **490**, 879–882.

Stern, S.A., W.B. McKinnon, and L.I. Lunine 1997. On the Origin of Pluto, Charon and the Pluto–Charon Binary. In *Pluto and Charon* (S.A. Stern and D.J. Tholen, eds.), University of Arizona Press, Tucson, pp. 605.

Stewart, G.R., and S. Ida 2000. Velocity Evolution of Planetesimals: Unified Analytical Formulas and Comparisons with N-Body Simulations. *Icarus* **143**, 28–44.

Sykes, M.V. 1990. Zodiacal Dust Bands - Their Relation to Asteroid Families. *Icarus* **85**, 267–289.

Tremaine, S. 1998. Resonant Relaxation in Protoplanetary Disks. *Astron. J.* **116**, 2015–2022.

Wetherill, G.W., and G.R. Stewart 1989. Accumulation of a Swarm of Small Planetesimals. *Icarus* **77**, 330–357.

Wetherill, G.W., and G.R. Stewart 1993. Formation of Planetary Embryos: Effects of Fragmentation, Low Relative Velocity, and Independent Variation of Eccentricity and Inclination. *Icarus* **106**, 190–209.

Weidenschilling, S.J., and J.N. Cuzzi 1993. Formation of Planetesimals in the Solar Nebula. In *Protostars and Planets III* (E.H. Levy and J.I. Lunine, Eds.), pp. 1031–1060. Univ. of Arizona Press, Tucson.

Weidenschilling, S.J., D. Spaute, D.R. Davis, F. Marzari, and K. Ohtsuki 1997. Accretional Evolution of a Planetesimal Swarm. 2. The Terrestrial Zone. *Icarus* **128**, 429–455.

Wisdom, J, and M. Holman 1991. Symplectic Maps for the N-Body Problem. *Astron. J.* **102**, 1528–1538.

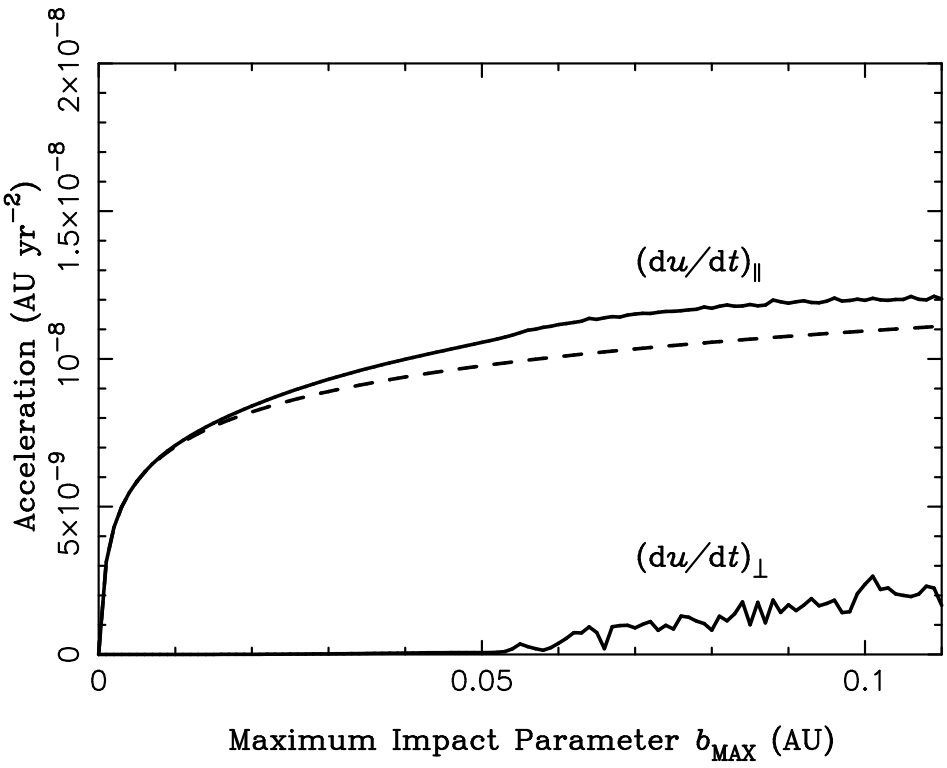

Fig. 1.— Magnitudes of the parallel $(\frac{d\vec{u}}{dt})_{\parallel}$ and transversal components $(\frac{d\vec{u}}{dt})_{\perp}$ of the acceleration. Solid lines show the accelerations evaluated numerically. The dashed line shows $(\frac{d\vec{u}}{dt})_{\parallel}$ computed analytically using the Taylor series approximation ($(\frac{d\vec{u}}{dt})_{\perp} = 0$ in this case). This figure and our other tests show that it is generally ok to account for $(\frac{dw}{dt})_{\parallel}$ only, use the analytic approximation, and take $b_{\rm MAX}$ to be several Hill radii of the perturbed massive body –here Earth– assuming the disk of small bodies extends so far.

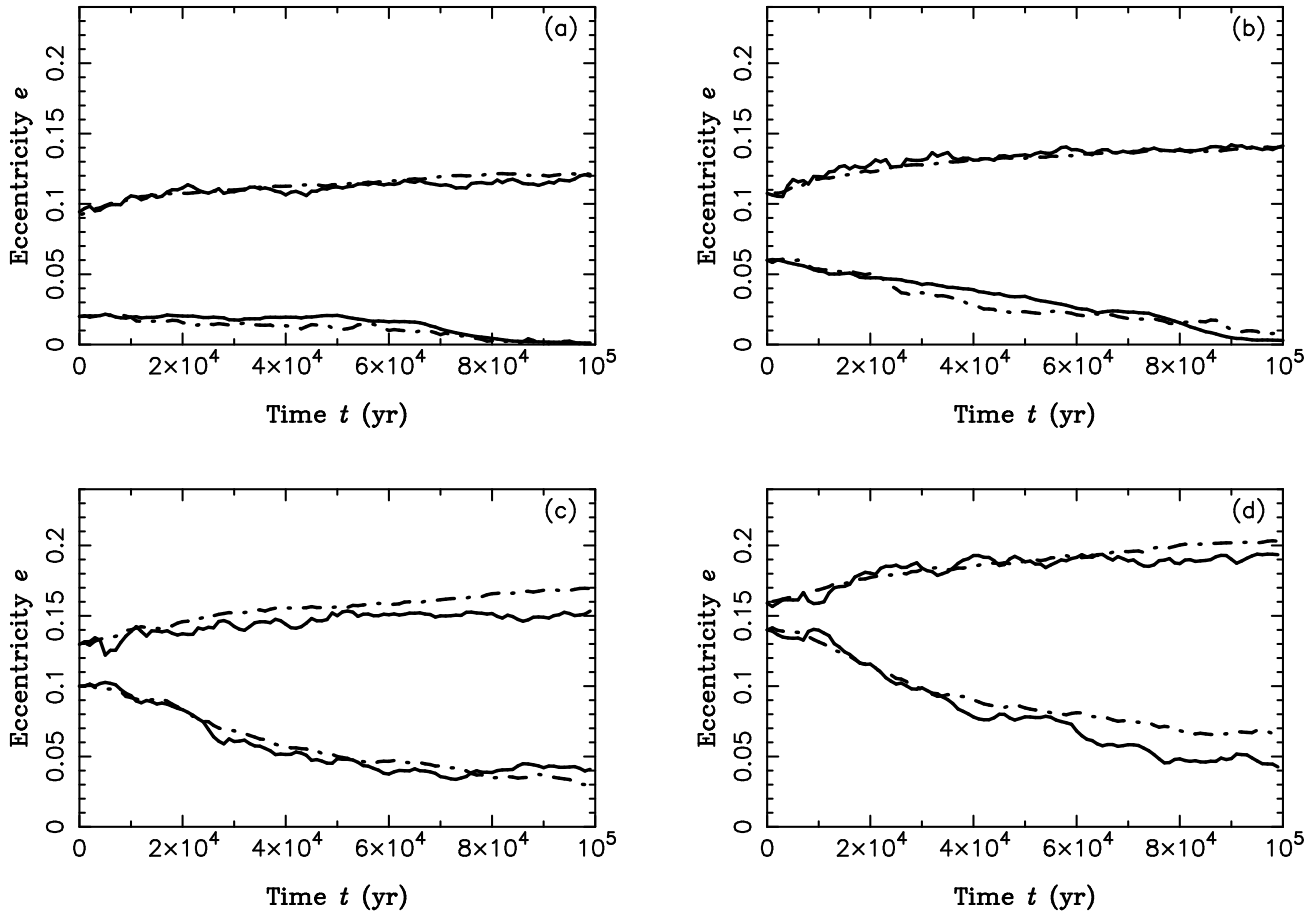

Fig. 2.— Comparison between the test (solid lines) and reference (dash-dotted lines) evolutions when the long-distance interactions between a protoplanet and planetesimals were neglected. In these experiments, an 1 $M_\oplus$ protoplanet at 1 AU is embedded in a planetesimal disk extending from 0.95 to 1.05 AU. The test (reference) evolutions were followed by the DFC1 (SyMBA) where the disk was resolved by 100 tracer particles (1000 point-mass disk particles). The total mass in the disk was 1 $M_\oplus$. From left-top panel to right-bottom panel we increased the initial e of the protoplanet: (a) $e = 0.02$, (b) $e = 0.06$, (c) $e = 0.1$, and (d) $e = 0.14$. All panels show a good agreement between the test and reference cases.

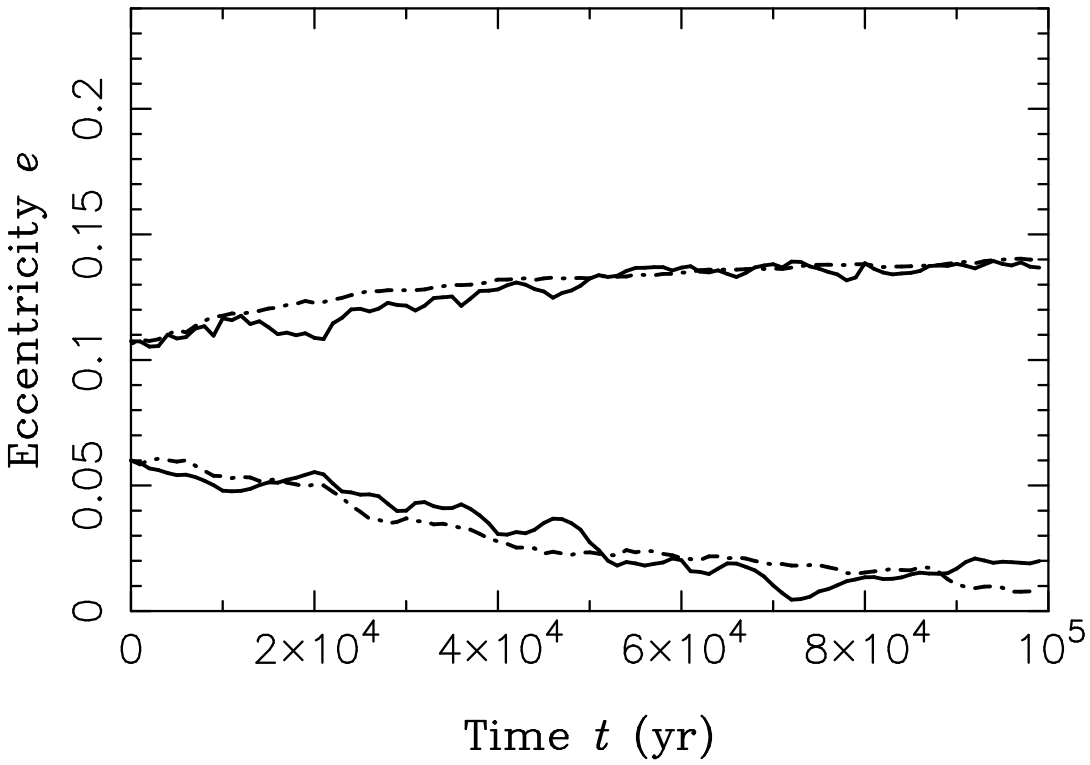

Fig. 3.— The same as Fig. 2b (initial protoplanet's $e = 0.06$), but this time the test evolution of the system was followed by the DFC2. Again, the agreement is good showing that the DFC2 with hundred tracers can correctly capture all important aspects of the dynamical evolution of the system.

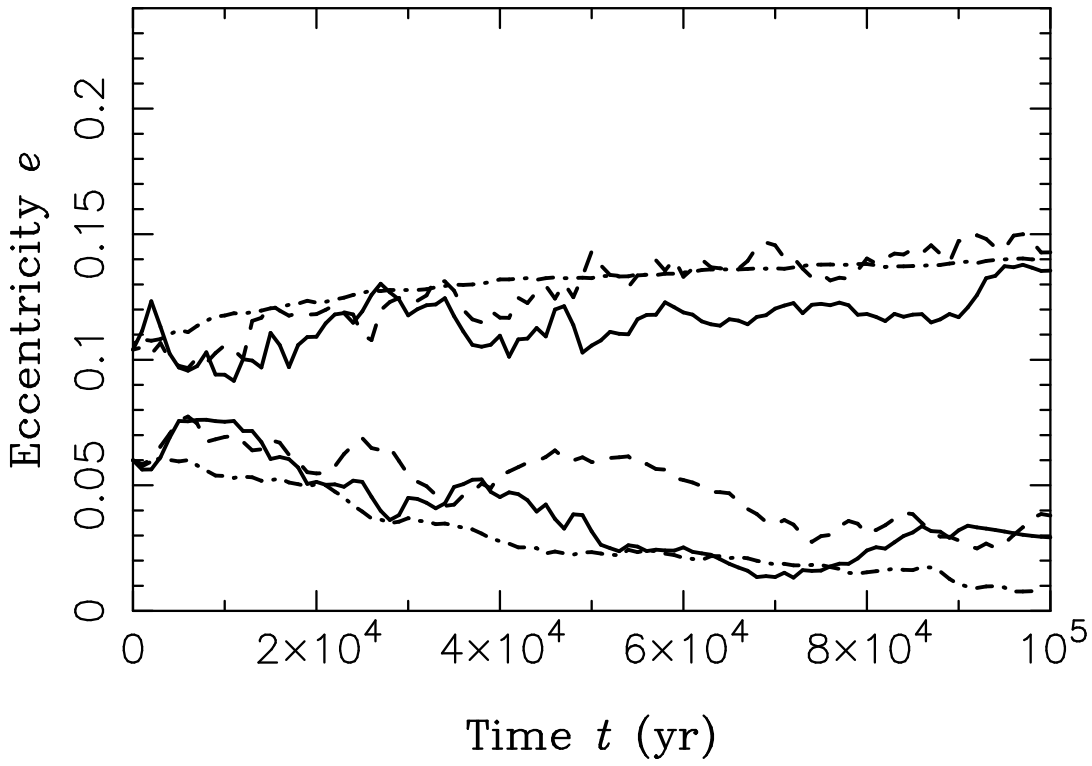

Fig. 4.— The same as Fig. 2b (initial protoplanet's $e = 0.06$), but when only twenty tracers were used to resolve the disk with the DFC1 (solid line) and the DFC2 (dashed line). The dash-dotted line shows the reference evolution where the SyMBA and 1000 point-mass disk particles were used. Though the test evolutions are not as smooth as the reference one, their general trends are similar resulting in a significant decay (increase) of the protoplanet's (planetesimals') e over 10^5 years.

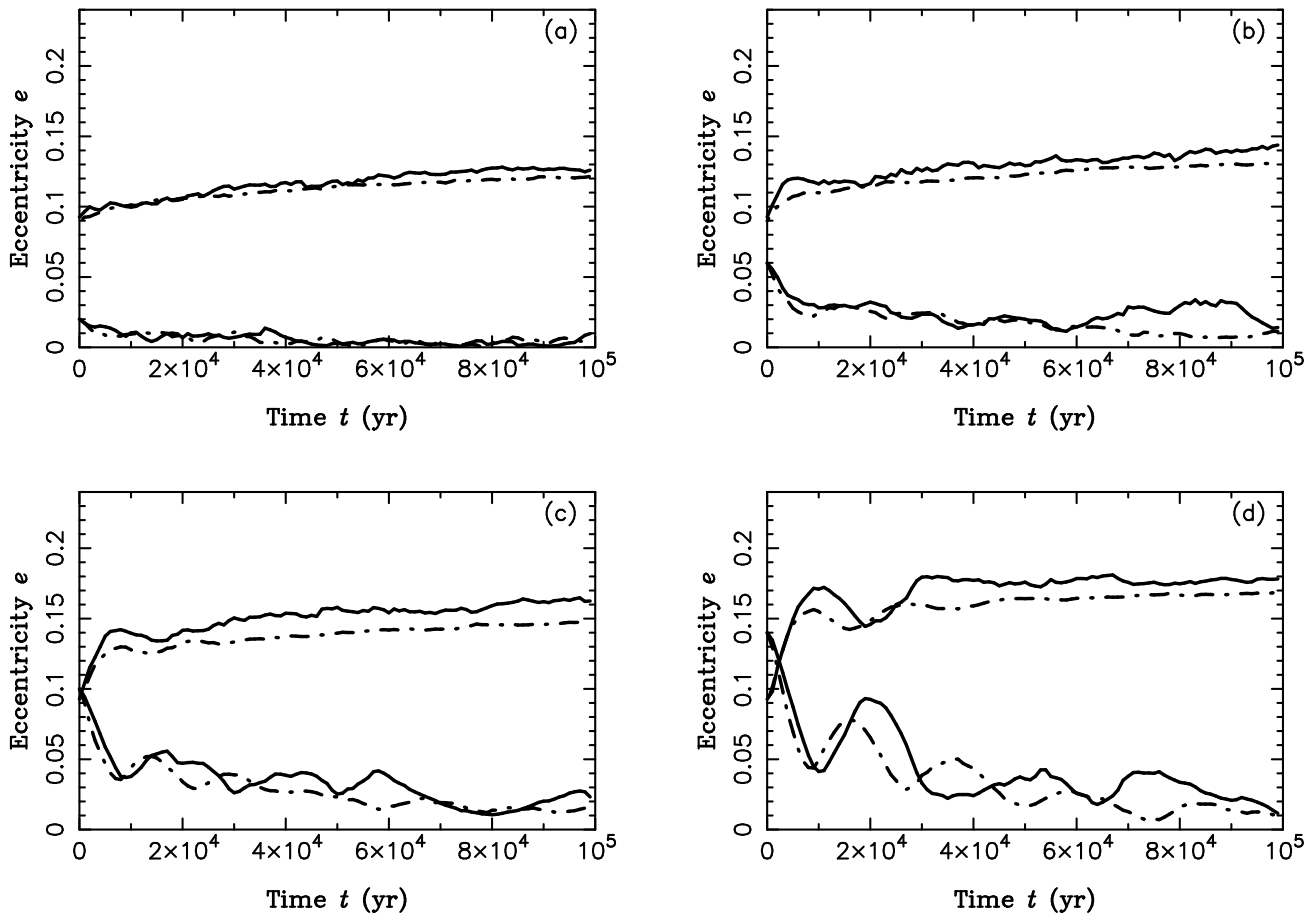

Fig. 5.— Comparison between test (solid lines) and reference (dash-dotted lines) evolutions. Unlike in Fig. 2, we accounted here for the full interaction of the protoplanet with the disk. In these experiments, the 1 $M_\oplus$ protoplanet at 1 AU was embedded in the planetesimal disk extending from 0.95 to 1.05 AU. The test (reference) evolutions were followed using the DFC1 (SyMBA). The disk was resolved by 100 tracer particles in the DFC1 and by 1000 point-mass disk particles in the SyMBA. The total mass in the disk was 1 $M_\oplus$. From left-top panel to right-bottom panel we increased the initial e of the protoplanet: (a) $e = 0.02$, (b) $e = 0.06$, (c) $e = 0.1$, and (d) $e = 0.14$. All panels show good agreement between the test and reference cases.

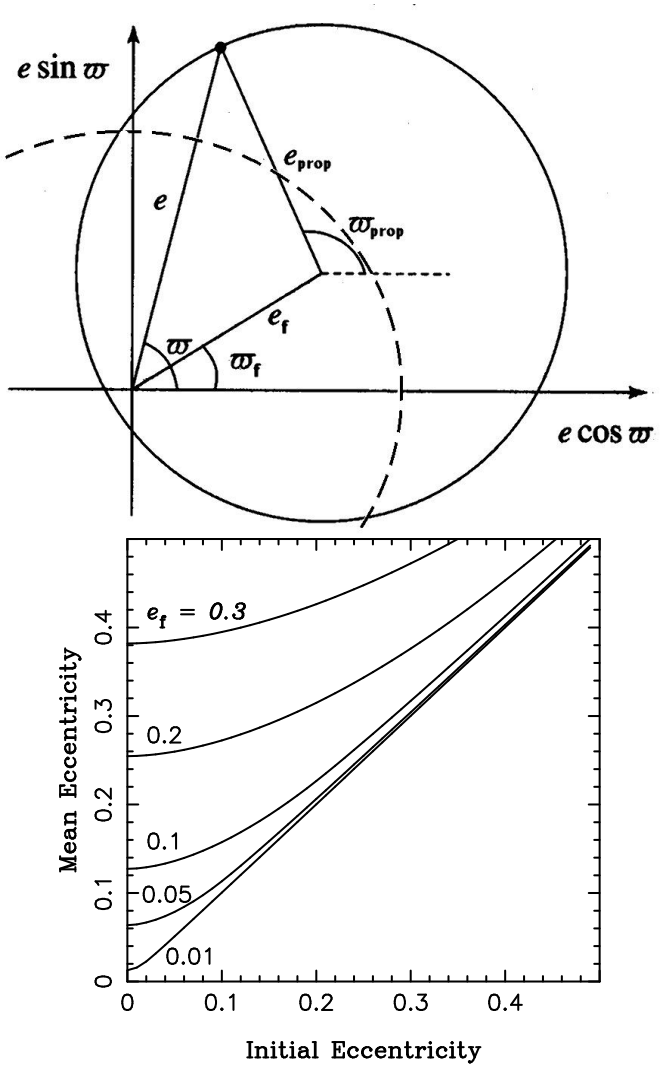

Fig. 6.— (a) Diagram that illustrates the secular friction. The secular motion of e and ϖ of a planetesimal can be represented by a vector of $e_{\rm prop}$ length in the $e\cos\varpi, e\sin\varpi$ plane that rotates with a constant angular speed around $(e_{\rm f}\cos\varpi_{\rm f}, e_{\rm f}\sin\varpi_{\rm f})$, where $e_{\rm f}$ and $\varpi_{\rm f}$ are the 'forced' eccentricity and periapse longitude (e.g., Murray & Dermott 1999). Without the forcing term (i.e., $e_{\rm f} = 0$), planetesimals would evolve along the dashed circle with radius that is equal to their eccentricity. With $e_{\rm f} \neq 0$ (i.e., when a protoplanet forms in the disk), these planetesimals evolve to larger (average) e because $e_{\rm f}$ is vectorially added to their secular motion. (b) The average final eccentricty of planetesimals as a function of their initial eccentricity for $e_{\rm f} = 0.01$, 0.05, 0.1, 0.2, and 0.3. The average final eccentricity is larger than the initial e in all cases. For this reason, when a protoplanet forms in a planetesimal disk, orbits of planetesimals evolve to larger e. By reaction, protoplanet's e decays.

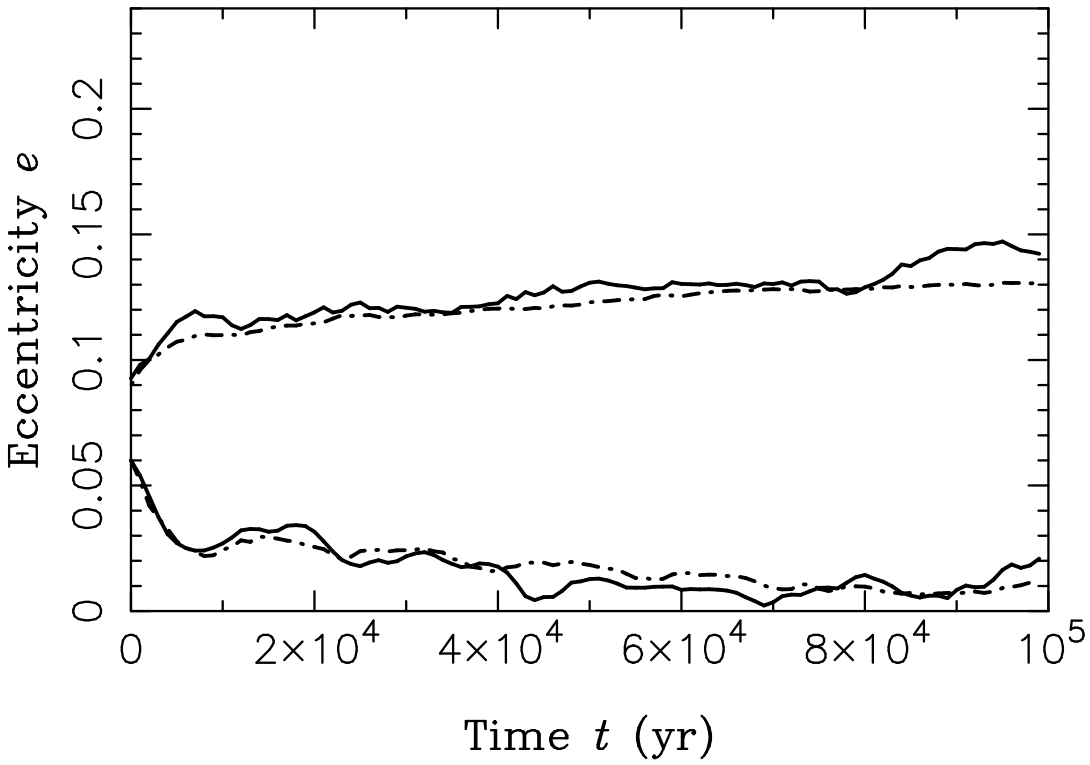

Fig. 7.— The same as Fig. 5b (initial protoplanet's $e = 0.06$), but this time the test evolution of the system was followed by the DFC2. Again, the agreement is good showing that the DFC2 with hundred tracers can correctly capture all important aspects of the dynamical evolution of the system.

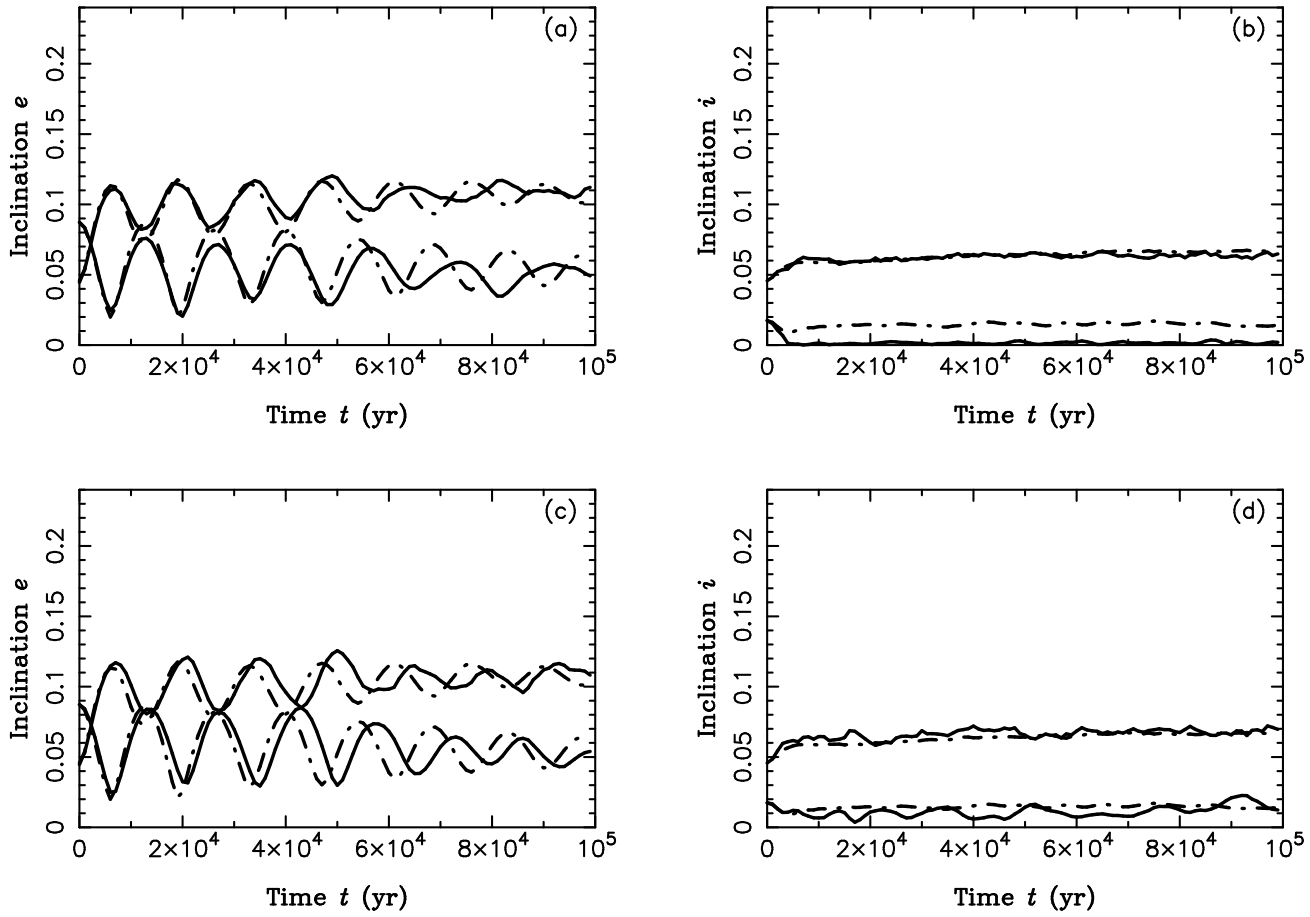

Fig. 8.— Comparison between the test (solid lines) and reference (dash-dotted lines) evolutions. In these tests, an 1 $M_\oplus$ protoplanet at 1 AU was embedded in a planetesimal disk that extends from 0.95 to 1.05 AU. The test (reference) evolutions were followed by the DFC1 & 2 (SyMBA). The planetesimal disk was resolved by 100 tracer particles in the DFC1 & 2 and by 1000 point-mass disk particles in the SyMBA. The total mass of the disk was 1 $M_\oplus$. We accounted for the gravitational perturbations by a Jupiter-mass planet at 5.2 AU. We used two different initial inclinations for the protoplanet: (a) & (c) $i = 5°$, (b) & (d) $i = 1°$. Test evolutions in top panels ((a) & (b)) were calculated using DFC1; the ones in the bottom panels ((c) & (d)) were calculated with the DFC2. All panels show good agreement between the test and reference cases, except (b) where the protoplanet's i decays to near-zero values when the DFC1 was used.

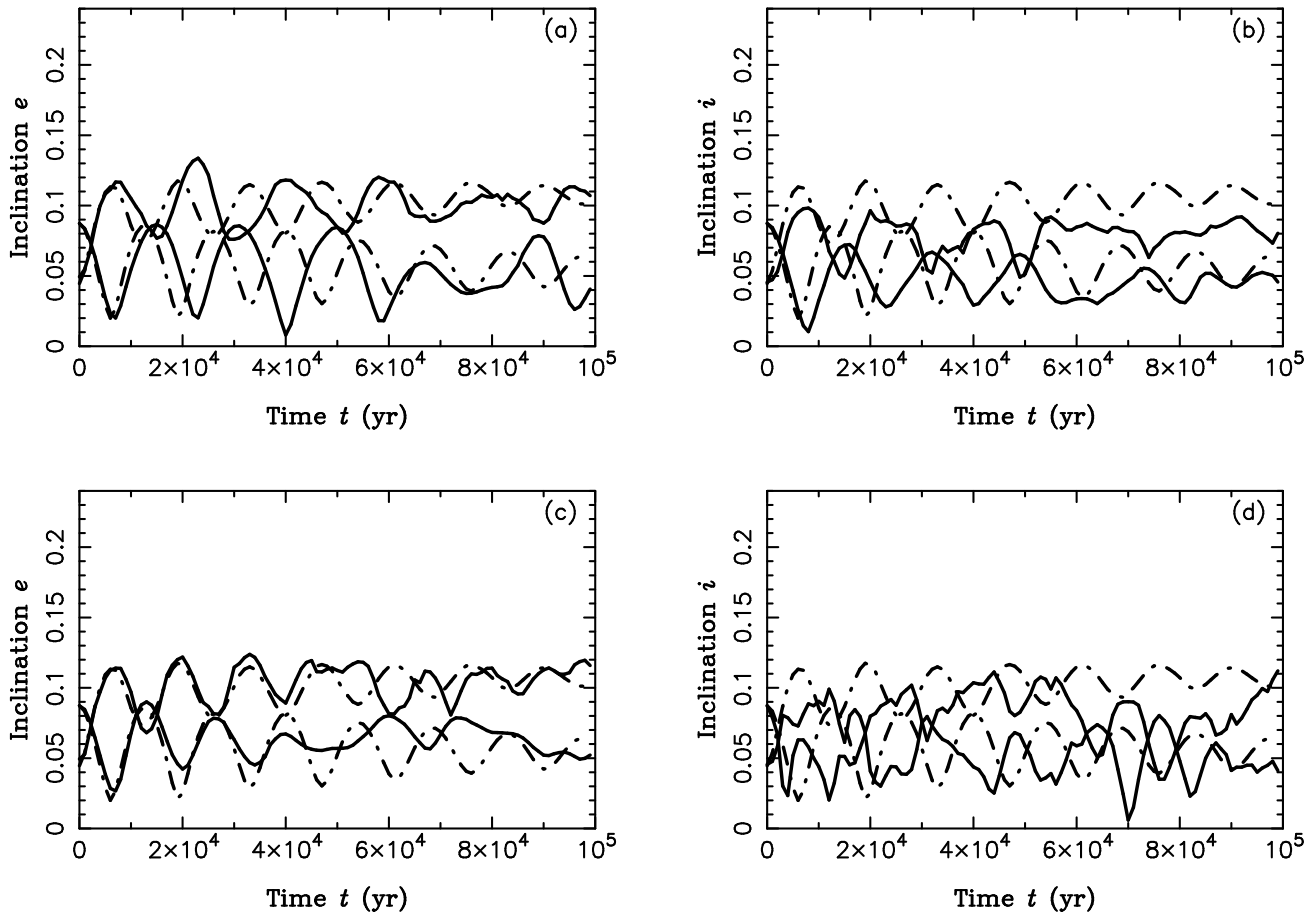

Fig. 9.— The same as Fig. 8, but with 20 (left panels) and 5 tracers (right panels) representing the 1 $M_\oplus$ disk at 0.95–1.05 AU. In (a) & (b), the test evolutions were computed using the DFC1. In (c) & (d), the test evolutions were computed using the DFC2. With 20 tracers, these test show evolutionary trends that are similar to the reference one; the test evolutions become very irregular with only five tracers.

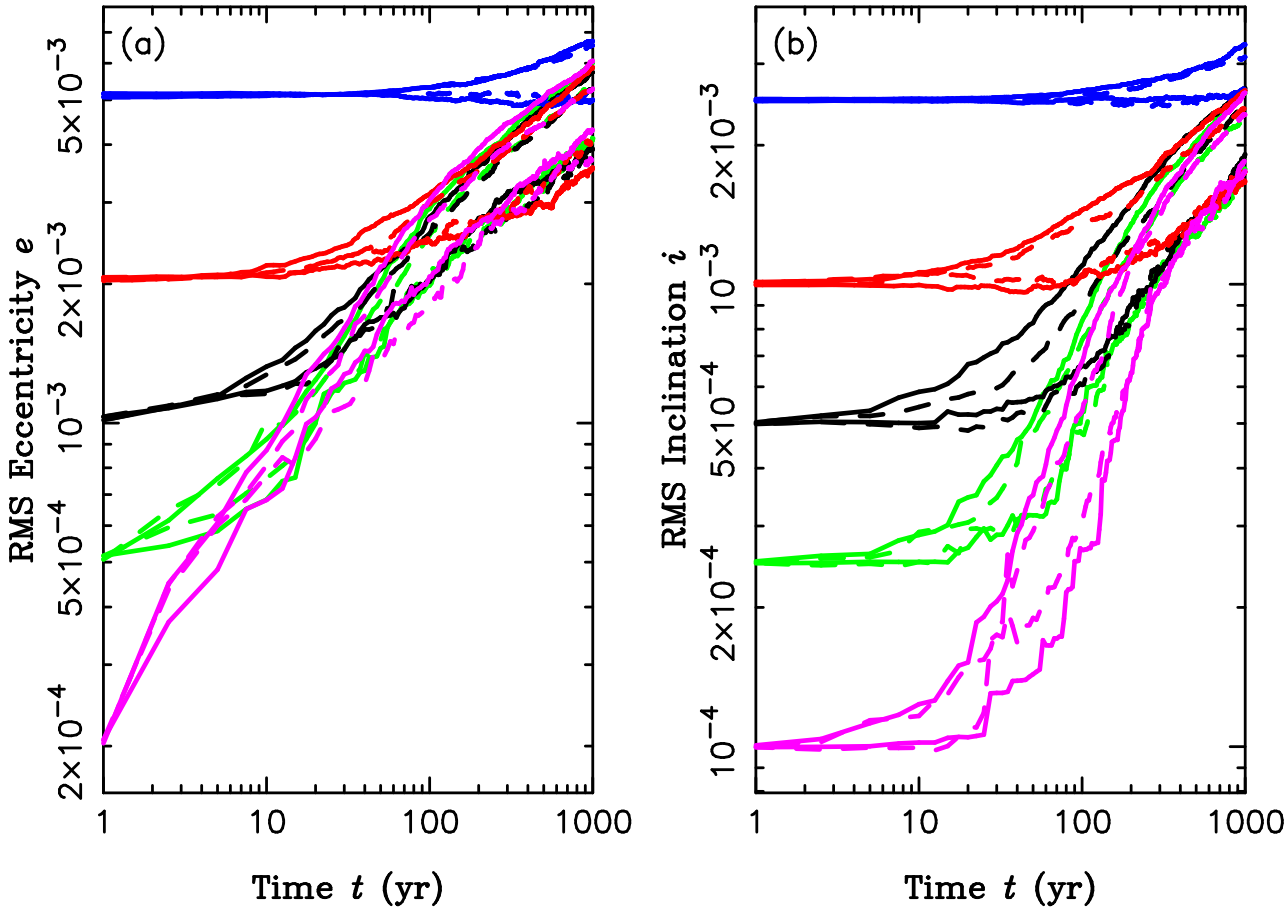

Fig. 10.— Comparison between the DFC1 and the exact N-body integrator SyMBA. Figure shows the evolutions of (a) $\sqrt{\langle e^2 \rangle}$ and (b) $\sqrt{\langle i^2 \rangle}$ computed using the DFC1 (solid lines) and the SyMBA (dashed lines) for five initial values of $\sqrt{\langle e^2 \rangle}$ (initial $\sqrt{\langle i^2 \rangle} = 0.5\sqrt{\langle e^2 \rangle}$ in all cases). The pairs of evolution paths started at $\sqrt{\langle e^2 \rangle} = 2 \times 10^{-4}$, 5×10^{-4}, 10^{-3}, 2×10^{-3}, and 5×10^{-3} show the RMS values $\sqrt{\langle e^2 \rangle}$ and $\sqrt{\langle i^2 \rangle}$ for big (bottom line in each pair) and small planetesimals (top lines). The agreement between the test and reference evolution paths is good. The DFC1 correctly follows the dynamical evolution of this system.

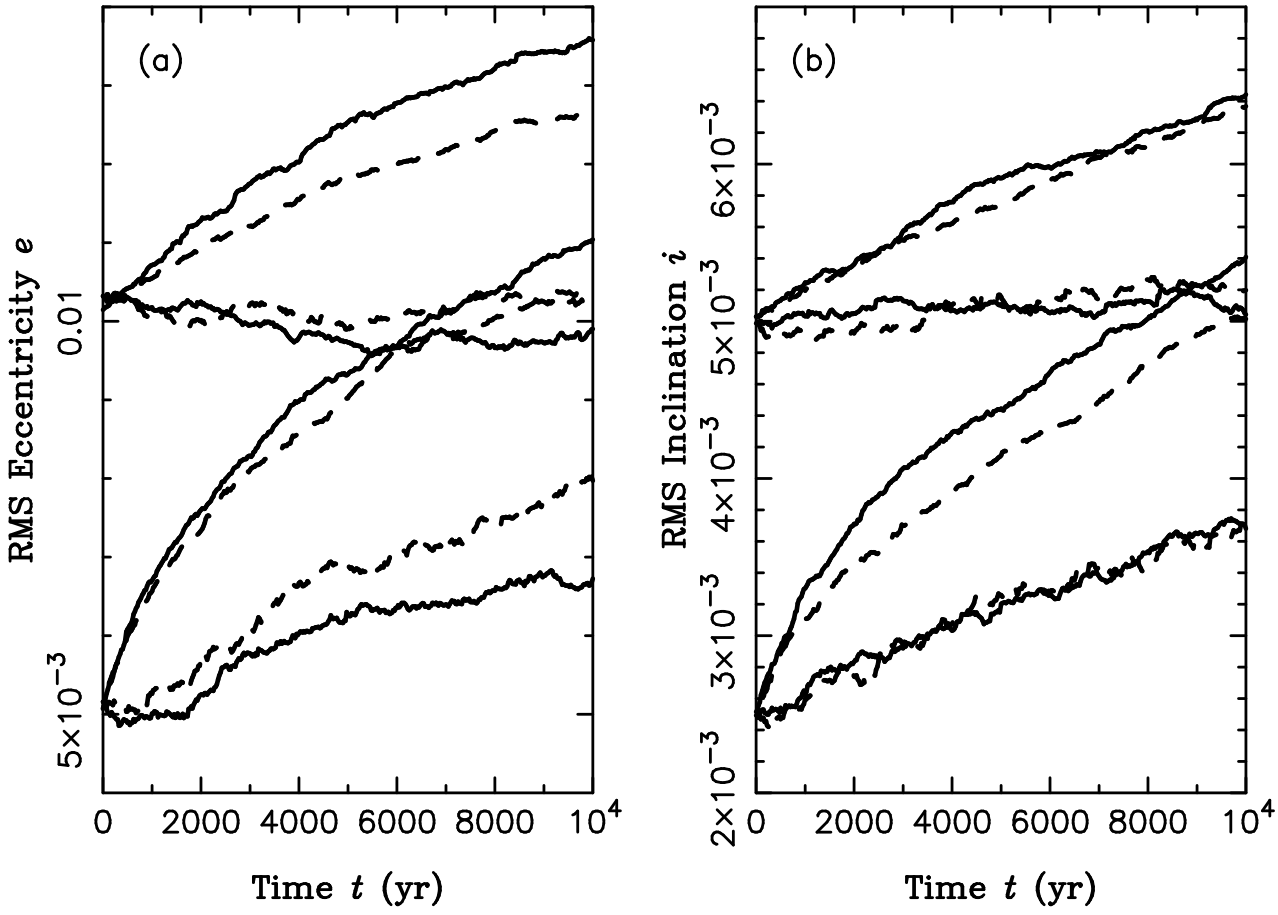

Fig. 11.— Comparison between the DFC1 and the exact N-body integrator SyMBA in a case of dispersion-dominated disks (example adapted from Ohtsuki et al. 2002). Figure shows evolutions of (a) $\sqrt{\langle e^2 \rangle}$ and (b) $\sqrt{\langle i^2 \rangle}$ (b) computed using the DFC1 (solid lines) and the SyMBA (dashed lines) for two initial values of $\sqrt{\langle e^2 \rangle}$ (initial $\sqrt{\langle i^2 \rangle} = 0.5\sqrt{\langle e^2 \rangle}$ in all cases). The pairs of evolution paths started at $\sqrt{\langle e^2 \rangle} = 5 \times 10^{-3}$ and 10^{-2} show the RMS values $\sqrt{\langle e^2 \rangle}$ and $\sqrt{\langle i^2 \rangle}$ for big (bottom line in each pair) and small planetesimals (top lines). The agreement between the test and reference evolution paths is satisfactory.